

Sliding Mode Control With Sliding Perturbation Observer

Jairo Terra Moura
Graduate Student.

Hakan Elmali
Visiting Assistant
Professor.

Nejat Olgac
Professor.

Department of Mechanical
Engineering U-139,
University of Connecticut,
Storrs, CT 06269

This work introduces a new robust motion control algorithm using partial state feedback for a class of nonlinear systems in the presence of modelling uncertainties and external disturbances. The effects of these uncertainties are combined into a single quantity called perturbation. The major contribution of this work comes as the development and design of a robust observer for the state and the perturbation which is integrated into a Variable Structure Controller (VSC) structure. The proposed observer combines the procedures of Sliding Observers (Slotine et al., 1987) with the idea of Perturbation Estimation (Elmali and Olgac, 1992). The result is what is called Sliding Perturbation Observer (SPO). The VSC follows the philosophy of Sliding Mode Control (SMC) (Slotine and Sastry, 1983). This combination of controller/observer gives rise to the new routine called Sliding Mode Control with Sliding Perturbation Observer (SMCSPO). The stability analysis shows how the algorithm parameters are scheduled in order to assure the sliding modes of both controller and observer. A simplified form of the general design procedure is also presented in order to ease the practical applications of SMCSPO. Simulations are presented for a two-link manipulator to verify the proposed approach. Experimental validation of the methodology is also performed on a PUMA 560 robot. A superior control performance is obtained over some full state feedback techniques such as SMC and Computed Torque Method.

1 Introduction

Sliding Mode Control (SMC) is a well-known technique due to its outstanding robustness properties against parametric uncertainties and external disturbances. Conventional SMC implementation utilizes the upper bound of each uncertainty to assure stability (Slotine and Sastry, 1983). This procedure typically yields over conservative control gains which limits tracking accuracy (Moura et al., 1995). As an improvement (Elmali and Olgac, 1992) introduces the concept of perturbation estimation in SMC, which results in a procedure called Sliding Mode Control with Perturbation Estimation (SMCPE). Perturbation vector is defined as the combined effect of all the uncertainties and external disturbances, the estimation of which constitutes a real time compensation mechanism against uncertainties. The accuracy of the estimation is the critical parameter for robustness in this scheme, as opposed to the upper bounds of the perturbations themselves. Consequently, the driving terms of the error dynamics are reduced from the uncertainties (as in the conventional SMC) to the accuracy in their estimates. The result is a much better tracking accuracy without being over conservative in control.

SMCPE opens an interesting research avenue: design of perturbation observers for SMC. Robust perturbation observers should be highly accurate within the frequency range of interest. The proper choice of observers can improve the tracking accuracy substantially (Jezernik et al., 1994). So far this perspective has received little attention in the literature due to the cost of the requirements of high quality sensor and full state feedback, which are essential to arrive at competitive performance levels. Another issue, which remains to be addressed, is the closed-loop stability of the sliding controller with perturbation observer. In (Elmali and Olgac, 1992), the perturbation estimation procedure is based on simple numerical differentiation of the state vector, which has certain limitations in the estimation phase. For instance, the applications with noisy velocity feedback requires

filtering operations in this procedure, restricting the tracking performance.

Sliding observer (SO) is a high performance state estimator well suited for nonlinear uncertain systems (Slotine et al., 1987) with partial state feedback. The sliding function of this observer is the estimation error of the available output. The basic SO structure consists of switching terms added to a conventional Luenberger observer (Luenberger, 1965).

The present work proposes the use of the SO as a tool to eliminate the requirement of a full state feedback in the perturbation estimation, reducing the implementation costs. Also, we show that the integration of perturbation estimation into the SO structure can substantially reduce the driving terms of the state observer error dynamics. Consequently, the resulting observer is able to provide much better state estimation accuracy. The combination of perturbation estimation and SO is named Sliding Perturbation Observer (SPO). We show that the further combination of this SPO and SMC results in a high performance algorithm that is robust against perturbations, utilizes only partial state feedback and outperforms conventional SMC with full state feedback and perfect measurements. This new algorithm is named as Sliding Mode Control with Sliding Perturbation Observer (SMCSPO) which forms the highlights of this paper. The stability analysis for the combination of the controller and the observer is presented for completeness. A systematic design procedure is offered taking into account the limitations of the control hardware. The approach is presented for general second order multi-degree of freedom systems. The extension of this procedure to a general order system is under current investigation.

The document is prepared as follows. Section 2 presents the system model and outlines the concept of perturbation. Section 3 reviews the SO approach. Sections 4, 5, and 6 are the major contributions of this work, where: Section 4 introduces the SPO, Sections 5 and 6 present SMCSPO algorithm with a stability proof for partial state feedback. Section 6 also presents a design procedure. Section 7 compares conventional SMC with SMCSPO. Section 8 verifies the proposed approach through simulations. Section 9 presents an experimental comparison among the SMCSPO, Computed Torque Method (CTM) and

Contributed by the Dynamic Systems and Control Division for publication in the JOURNAL OF DYNAMIC SYSTEMS, MEASUREMENT, AND CONTROL. Manuscript received by the DSCD June 1996. Associate Technical Editor: V. Utkin.

conventional SMC (with full state feedback). Section 10 concludes the work.

2 System Modeling and the Perturbation Concept

This section presents the system dynamics which is taken into account along with the definition of perturbation (Elmali and Olgac, 1992). The governing equation for general second order dynamics with n -degree-of-freedom (dof) is:

$$\ddot{x}_j = f_j(\mathbf{x}) + \Delta f_j(\mathbf{x}) + \sum_{i=1}^n [(b_{ji}(\mathbf{x}) + \Delta b_{ji}(\mathbf{x}))u_i] + d_j(t), \quad j = 1, \dots, n \quad (1)$$

where $\mathbf{x} \triangleq [X_1 \dots X_n]^T$ is the state vector and $\mathbf{X}_j \triangleq [x_j \dot{x}_j]^T$. The terms $f_j(\mathbf{x})$ and $\Delta f_j(\mathbf{x})$ correspond to the nonlinear driving terms and their uncertainties. The components b_{ij} and Δb_{ij} represent the elements of the control gain matrix and their uncertainties, while d_j is the external disturbance and u_j is the control input. The terms f_j and b_{ji} are known continuous functions of the state.

Perturbation is defined as the combination of all the uncertainties of Eq. (1):

$$\Psi_j(\mathbf{x}, t) = \Delta f_j(\mathbf{x}) + \sum_{i=1}^n [\Delta b_{ji}(\mathbf{x})u_i] + d_j(t). \quad (2)$$

The control task is to drive the state \mathbf{x} towards a desired state $\mathbf{x}_d \triangleq [X_{1d} \dots X_{nd}]^T$ despite these perturbations. It is assumed that the perturbations are upper bounded by a known continuous function of the state (Elmali and Olgac, 1992):

$$\Gamma_j(\mathbf{x}, t) = F_j(\mathbf{x}) + \sum_{i=1}^n |\Phi_{ji}(\mathbf{x})u_i| + D_j(t) > |\Psi_j(t)| \quad (3)$$

where $F_j > |\Delta f_j|$, $\Phi_{ji} > |\Delta b_{ji}|$ and $D_j > |d_j|$ represent the expected upper bounds of the uncertainties.

3 Sliding Observer for Single Input Single Output (SISO) Systems

A brief review of SO is presented next for a SISO system, following (Slotine et al., 1987). SO is a robust observer structure which estimates the state of a non-linear uncertain system. The state space representation of a second order single dof system is:

$$\begin{aligned} \dot{x}_1 &= x_2 \\ \dot{x}_2 &= f(\mathbf{x}) + bu + \Delta f(\mathbf{x}) + \Delta bu + d(t) \\ y &= x_1 \end{aligned} \quad (4)$$

where $\mathbf{x} = [x_1 \ x_2]^T$ is the state vector and x_1 is assumed to be the only measurable state. The observer task is to estimate the state \mathbf{x} despite the uncertainties. The SO structure is presented next:

$$\begin{aligned} \dot{\hat{x}}_1 &= \hat{x}_2 - k_1 \operatorname{sgn}(\hat{x}_1) - \alpha_1 \hat{x}_1 \\ \dot{\hat{x}}_2 &= f(\hat{\mathbf{x}}) + bu - k_2 \operatorname{sgn}(\hat{x}_1) - \alpha_2 \hat{x}_1 \end{aligned} \quad (5)$$

where $k_1, k_2, \alpha_1, \alpha_2$ are positive numbers and $\hat{x}_1 = \hat{x}_1 - x_1$ is the estimation error of the measurable state. Throughout the text, “ $\hat{\cdot}$ ” refers to estimation errors whereas “ $\hat{\cdot}$ ” symbolizes the estimated quantity. Using (4) and (5) the resulting estimation error dynamics are

$$\begin{aligned} \dot{\hat{x}}_1 &= \hat{x}_2 - k_1 \operatorname{sgn}(\hat{x}_1) - \alpha_1 \hat{x}_1 \\ \dot{\hat{x}}_2 &= -k_2 \operatorname{sgn}(\hat{x}_1) - \alpha_2 \hat{x}_1 - \Psi \end{aligned} \quad (6)$$

where Ψ is defined in (2) and the difference $\hat{f} = f(\hat{\mathbf{x}}) - f(\mathbf{x})$ is assumed to be part of the uncertainty Δf of expression (2). The observer sliding mode takes place on the line $\hat{x}_1 = 0$ of the

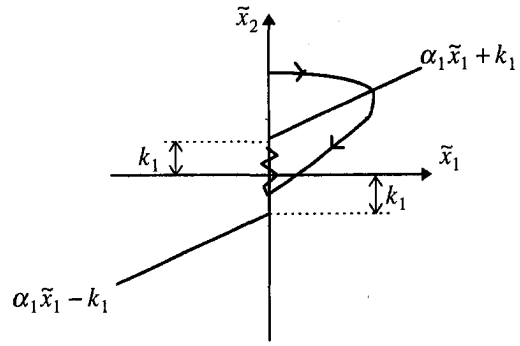


Fig. 1 Observer state space and sliding mode

observer state space \hat{x}_1 vs. \hat{x}_2 . Figure 1 depicts a typical state space trajectory. The conditions for the existence of sliding mode are

$$\begin{aligned} \hat{x}_2 &\leq k_1 + \alpha_1 \hat{x}_1 \quad (\text{if } \hat{x}_1 > 0) \\ \hat{x}_2 &\geq -k_1 + \alpha_1 \hat{x}_1 \quad (\text{if } \hat{x}_1 < 0). \end{aligned} \quad (7)$$

Once the sliding takes place (i.e. $\hat{x}_1 = 0$) the resulting error dynamics take the form

$$\dot{\hat{x}}_2 + (k_2/k_1)\hat{x}_2 = -\Psi. \quad (8)$$

Note that (8) is a filter between Ψ and \hat{x}_2 with a cut-off frequency at k_2/k_1 . It is desirable to place the break point k_2/k_1 as high as possible in order to maximize the attenuation from Ψ to \hat{x}_2 , and consequently improve the estimation accuracy of x_2 . The choice of k_2/k_1 is discussed in Section 6.

The stability of the SO is guaranteed by setting $k_2 \geq \Gamma(\mathbf{x}, t)$, which assures in steady state $|\hat{x}_2| \leq k_1$ as can be seen from (8) implying that the sliding conditions (7) are also verified. The expression for k_2 should be based on $\hat{\mathbf{x}}$ (not on \mathbf{x}). We assume that $\Gamma(\hat{\mathbf{x}}, t)$ is also an upper bound of Ψ , meaning that the uncertainties due to state estimation are negligible compared to the modeling uncertainties and external disturbances. This is a reasonable assumption since the estimation errors can be reduced by increasing k_2/k_1 independently from Ψ . Therefore, the selection for k_2 is made as

$$k_2 = \Gamma(\hat{\mathbf{x}}, t). \quad (9)$$

4 Sliding Perturbation Observer (SPO)

This section introduces the proposed perturbation observer without considering the closed-loop control. In 4.1, a new control variable is defined in order to decouple the control of Eq. (1). This simplifies the formulation as will be described later. 4.2 presents a simple perturbation observer structure similar to Jezernik et al. (1994). Finally, 4.3 shows that the combination of perturbation and sliding observers results in a more effective observer structure: Sliding Perturbation Observer (SPO). We note again that, throughout this section we focus on stabilizing the observer dynamics without the presence of a closed loop control.

4.1 Control Variable Transformation. Before integrating SO into SMC it is convenient to decouple the control variable using the following transformation:

$$f_j(\hat{\mathbf{x}}) + \sum_{i=1}^n b_{ji}(\hat{\mathbf{x}})u_i = \alpha_{3j}\bar{u}_j \quad (11)$$

where α_{3j} is an arbitrary positive number and \bar{u}_j is the new control variable. The original control vector of Eq. (1) is easily obtained as

$$\mathbf{u} = \mathbf{B}^{-1} \text{Col} [\alpha_{3j} \bar{u}_j - f_j(\hat{\mathbf{x}})] \quad (12)$$

where $\mathbf{u} = [u_1 \dots u_n]^T$ and $\mathbf{B} = [b_{ji}(\hat{\mathbf{x}})]_{n \times n}$. The difference $b_{ji}(\hat{\mathbf{x}}) - b_{ji}(\mathbf{x})$ is considered as part of Δb_{ji} terms of expression (2).

Transformation (11) allows us to write the system dynamics as:

$$\dot{x}_j = \alpha_{3j} \bar{u}_j + \Psi_j. \quad (13)$$

The state space representation of (13) is

$$\begin{aligned} \dot{x}_{1j} &= x_{2j} \\ \dot{x}_{2j} &= \alpha_{3j} \bar{u}_j + \Psi_j \\ y_j &= x_{1j} \end{aligned} \quad (14)$$

and the corresponding SO structure is

$$\begin{aligned} \dot{\hat{x}}_{1j} &= \hat{x}_{2j} - k_{1j} \text{sgn}(\hat{x}_{1j}) - \alpha_{1j} \hat{x}_{1j} \\ \dot{\hat{x}}_{2j} &= \alpha_{3j} \bar{u}_j - k_{2j} \text{sgn}(\hat{x}_{1j}) - \alpha_{2j} \hat{x}_{1j}. \end{aligned} \quad (15)$$

The conditions for the existence of the observer sliding mode and stability are identical to (7) and (9), respectively, for each degree of freedom “ j ”.

4.2 Perturbation Observer. The development of a perturbation observer is presented next. Throughout this subsection full state feedback is assumed in order to focus on the perturbation estimation aspects of the strategy only. Section 4.3 addresses the issue of partial state feedback, with no x_{2j} measurements available.

Let x_{3j} be a new state variable defined as

$$x_{3j} = \alpha_{3j} x_{2j} - \Psi_j / \alpha_{3j}. \quad (16)$$

It is desirable to observe the variable x_{3j} and consequently calculate Ψ_j using this relation instead of estimating it directly, as was the case in Elmalı and Olgac (1992). In order to accomplish this, it is assumed that:

1. Ψ_j exists (i.e., there are only continuous perturbations) and it is bounded.
2. The spectrum of Ψ_j lies within a known finite frequency range λ_Ψ .

Note that assumption 1 does not hold for instants when discontinuities in the perturbation signal occur (e.g., dry friction at zero velocity points). Even the conventional SMC strategies with actuators of finite bandwidth could not counteract this type of perturbation at these instants. Therefore, assumption 1 does not introduce an additional constraint to those used commonly for SMC (Slotine and Sastry, 1983).

The time derivative of Eq. (16) gives

$$\dot{x}_{3j} = \alpha_{3j} \dot{x}_{2j} - \frac{\dot{\Psi}_j}{\alpha_{3j}}. \quad (17)$$

At this point we assume that it is possible to select an α_{3j} high enough so that the term $\dot{\Psi}_j / \alpha_{3j}$ can be neglected relative to $\alpha_{3j} \dot{x}_{2j}$. Based on this assumption and using (14) and (16), we propose the following observer equation for x_{3j} (and Ψ_j):

$$\begin{aligned} \dot{\hat{x}}_{3j} &= \alpha_{3j}^2 (-\hat{x}_{3j} + \alpha_{3j} x_{2j} + \bar{u}_j) \\ \hat{\Psi}_j &= \alpha_{3j} (-\hat{x}_{3j} + \alpha_{3j} x_{2j}) \end{aligned} \quad (18)$$

Using Eqs. (14), (17), and (18), the estimation error dynamics is obtained as

$$\dot{\tilde{x}}_{3j} = -\alpha_{3j}^2 \tilde{x}_{3j} + \dot{\Psi}_j / \alpha_{3j} \quad (19)$$

where $\tilde{x}_{3j} = \hat{x}_{3j} - x_{3j}$ is the estimation error. Note that we can write $\tilde{x}_{3j} = -\dot{\Psi}_j / \alpha_{3j}$ so that $\dot{\tilde{x}}_{3j} = -\alpha_{3j}^2 \tilde{x}_{3j} + \dot{\Psi}_j$, which in Laplace domain becomes

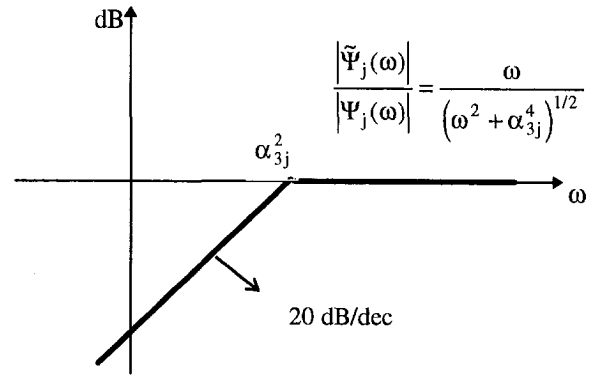


Fig. 2 Magnitude plot of the transfer function of Eq. (20)

$$\hat{\Psi}_j(p) = \frac{p}{p + \alpha_{3j}^2} \Psi_j(p). \quad (20)$$

Throughout this text, “ p ” represents the Laplace variable. Equation (20) is a high pass filter with input Ψ_j and output $\hat{\Psi}_j$, the perturbation estimation error. Figure 2 depicts its frequency magnitude plot. As can be seen, it is desirable to maximize the break point α_{3j}^2 in order to attenuate the lower frequency contents of the perturbation signal as much as possible. This is consistent with the assumptions that generated the observer equations. If α_{3j}^2 is placed higher than λ_Ψ then, in steady state, the upper bounds of $\hat{\Psi}_j$ become smaller than those of Ψ_j .

4.3 Sliding Perturbation Observer. This section introduces a perturbation observer that utilizes only partial state feedback (x_{1j} in this treatment). Consequently, it is necessary to estimate x_{2j} in order to obtain $\hat{\Psi}_j$. We propose a new observer structure that combines the SO of (15) with the perturbation observer of (18). The result is a better state observer that also provides an on-line perturbation estimation scheme using only partial state feedback. The idea is to use the perturbation estimate $\hat{\Psi}_j$ in the SO in order to reduce the driving terms of the error dynamics of (8). That is, instead of Ψ_j , $\hat{\Psi}_j = \hat{\Psi}_j - \Psi_j$ becomes the input to (8). Consequently, the estimation accuracy of x_{2j} improves at least to the order of the perturbation estimation accuracy. This new structure can be achieved by writing the observer equations (15) as:

$$\begin{aligned} \dot{\hat{x}}_{1j} &= \hat{x}_{2j} - k_{1j} \text{sgn}(\hat{x}_{1j}) - \alpha_{1j} \hat{x}_{1j} \\ \dot{\hat{x}}_{2j} &= \alpha_{3j} \bar{u}_j - k_{2j} \text{sgn}(\hat{x}_{1j}) - \alpha_{2j} \hat{x}_{1j} + \hat{\Psi}_j \\ \dot{\hat{x}}_{3j} &= \alpha_{3j}^2 (-\hat{x}_{3j} + \alpha_{3j} \hat{x}_{2j} + \bar{u}_j) \end{aligned} \quad (21)$$

where

$$\hat{\Psi}_j = \alpha_{3j} (-\hat{x}_{3j} + \alpha_{3j} \hat{x}_{2j}). \quad (22)$$

These equations constitute the Sliding Perturbation Observer. Note that Eqs. (21) couple the observers for states x_{2j} and x_{3j} in contrast to the earlier Eqs. (15) and (18) where state x_{2j} was considered to be available. The new observer error dynamics become

$$\begin{aligned} \dot{\tilde{x}}_{1j} &= \tilde{x}_{2j} - k_{1j} \text{sgn}(\hat{x}_{1j}) - \alpha_{1j} \tilde{x}_{1j} \\ \dot{\tilde{x}}_{2j} &= -k_{2j} \text{sgn}(\hat{x}_{1j}) - \alpha_{2j} \tilde{x}_{1j} + \tilde{\Psi}_j \\ \dot{\tilde{x}}_{3j} &= \alpha_{3j}^2 (-\tilde{x}_{3j} + \alpha_{3j} \tilde{x}_{2j}) + \dot{\tilde{\Psi}}_j / \alpha_{3j}. \end{aligned} \quad (23)$$

After the observer sliding mode begins, \tilde{x}_{2j} dynamics become

$$\dot{\tilde{x}}_{2j} + (k_{2j}/k_{1j}) \tilde{x}_{2j} = \tilde{\Psi}_j. \quad (24)$$

Note that the input of \tilde{x}_{2j} dynamics is reduced from Ψ_j (as in (8)) to $\tilde{\Psi}_j$ (in (24)). The transfer function between $\tilde{\Psi}_j$ and Ψ_j

can be obtained using (16) and the last of Eqs. (23). After simplifications it yields

$$\tilde{\Psi}_j(p) = \frac{p(p + k_{2j}/k_{1j})}{p^2 + (k_{2j}/k_{1j})p + (k_{2j}/k_{1j})\alpha_{3j}^2} (-\Psi_j(p)) \quad (25)$$

which is a high pass filter. Naturally the observer parameters involved are selected to attenuate the incoming perturbation signal within its expected frequency range. Section 6 describes this process in detail.

The relation between \tilde{x}_{2j} and Ψ_j is obtained from Eqs. (24) and (25) as

$$\tilde{x}_{2j}(p) = \frac{p}{p^2 + (k_{2j}/k_{1j})p + (k_{2j}/k_{1j})\alpha_{3j}^2} (-\Psi_j(p)). \quad (26)$$

Note that $\tilde{x}_{2j}(p)$ is desired to be small for better state estimation for x_{2j} . Hence the parameters k_{2j}/k_{1j} and α_{3j} must be selected to maximize the attenuation from perturbation $\Psi_j(p)$ to $\tilde{x}_{2j}(p)$.

4.4 Effect of Saturation Function. The above analysis of observer contains no feedback control scheme so far. Equations (8), (24), (25), and (26) are obtained assuming perfect observer sliding (i.e., $\tilde{x}_{1j} = 0$). As it is explained in later sections, when SPO is integrated into SMC strategy it is necessary to smooth the discontinuous $\text{sgn}(\tilde{x}_{1j})$ to eliminate the control chatter. Saturation functions are used instead, and they are defined as

$$\text{sat}(\tilde{x}_{1j}) = \begin{cases} \tilde{x}_{1j}/|\tilde{x}_{1j}|, & \text{if } |\tilde{x}_{1j}| \geq \epsilon_{oj} \\ \tilde{x}_{1j}/\epsilon_{oj}, & \text{if } |\tilde{x}_{1j}| \leq \epsilon_{oj} \end{cases} \quad (27)$$

where ϵ_{oj} is the boundary layer of the SPO.

Without disturbing the generality, we assume that at time $t = 0$ x_{1j} and x_{2j} are perfectly known so that $\tilde{x}_{1j}(0) = 0$, $\tilde{x}_{2j}(0) = 0$. That means, the observer starts on the sliding surface and always remains in the boundary layer provided that the gain k_{2j} is high enough (as described in Section 3). Thus all the $\text{sgn}(\tilde{x}_{1j})$ terms of previous equations can be replaced by $\tilde{x}_{1j}/\epsilon_{oj}$. Since reaching phase is already eliminated, the attractivity parameters α_{1j} and α_{2j} are selected to be zero. After these changes, the frequency domain relation between $\tilde{\Psi}_j$ and Ψ_j is modified to

$$\tilde{\Psi}_j(p) = \frac{p[p^2 + (k_{1j}/\epsilon_{oj})p + k_{2j}/\epsilon_{oj}]}{p^3 + (k_{1j}/\epsilon_{oj})p^2 + (k_{2j}/\epsilon_{oj})p + \alpha_{3j}^2 k_{2j}/\epsilon_{oj}} (-\Psi_j(p)) \quad (28)$$

which yields

$$\tilde{x}_{2j}(p) = \frac{p(p + k_{1j}/\epsilon_{oj})}{p^3 + (k_{1j}/\epsilon_{oj})p^2 + (k_{2j}/\epsilon_{oj})p + \alpha_{3j}^2 k_{2j}/\epsilon_{oj}} (-\Psi_j(p)). \quad (29)$$

For the sake of comparison the corresponding transfer function between \tilde{x}_{2j} and Ψ_j for SO is obtained by subtracting (15) and (14) which yields

$$\tilde{x}_{2j}(p) = \frac{p + k_{1j}/\epsilon_{oj}}{p^2 + (k_{1j}/\epsilon_{oj})p + k_{2j}/\epsilon_{oj}} (-\Psi_j(p)). \quad (30)$$

Further comparisons are presented in Section 6 between SO and SPO.

In Sections 3 and 4 above the emphasis has been on stabilizing the observers. In the following sections (5 and 6) a control strategy is appended to these observers and the stability of the combined dynamics is proven.

5 Sliding Mode Control With Sliding Perturbation Observer (SMCSPO)

This section presents the integration of SMC control law and SPO observer scheme. For the system of Eq. (14), we define the estimated sliding function as:

$$\hat{s}_j = \dot{e}_j + c_{j1} e_j \quad (31)$$

where $c_{j1} > 0$, $\hat{e}_j = \hat{x}_{1j} - x_{1dj}$ is the estimated position tracking error and $[x_{1dj} \ x_{1dj}]^T$ is the desired motion for the “ j -th” degree of freedom. The actual sliding function is

$$s_j = \dot{e}_j + c_{j1} e_j, \quad (32)$$

where $e_j = x_{1j} - x_{1dj}$ is the actual position tracking error.

The estimation error of the sliding function is defined as $\tilde{s}_j = \hat{s}_j - s_j$. Using Eqs. (21) and (23) its value can be computed as

$$\tilde{s}_j = \tilde{x}_{1j} + c_{j1} \tilde{x}_{1j}. \quad (33)$$

The control \bar{u}_j is selected to enforce $\tilde{s}_j \dot{\tilde{s}}_j < 0$ outside a prescribed manifold. A desired \hat{s}_j -dynamics is selected as

$$\dot{\hat{s}}_j = -K_j \text{sat}(\hat{s}_j) \quad (34)$$

where

$$\text{sat}(\hat{s}_j) = \begin{cases} \hat{s}_j/|\hat{s}_j|, & \text{if } |\hat{s}_j| \geq \epsilon_{cj} \\ \hat{s}_j/\epsilon_{cj}, & \text{if } |\hat{s}_j| \leq \epsilon_{cj} \end{cases} \quad (35)$$

is used due to its desirable anti-chatter properties (Slotine and Sastry, 1983). In this equation, ϵ_{cj} stands for boundary layer of the SMC controller, as opposed to the ϵ_{oj} in SPO.

Using the results of previous sections it is possible to compute $\dot{\hat{s}}_j$ as

$$\dot{\hat{s}}_j = \alpha_{3j} \bar{u}_j - [k_{2j}/\epsilon_{oj} + c_{j1}(k_{1j}/\epsilon_{oj}) - (k_{1j}/\epsilon_{oj})^2] \tilde{x}_{1j} - (k_{1j}/\epsilon_{oj}) \tilde{x}_{2j} - \dot{x}_{1dj} + c_{j1}(\hat{x}_{2j} - \dot{x}_{1dj}) + \tilde{\Psi}_j. \quad (36)$$

In order to enforce (34) when $\tilde{x}_{2j} = 0$, a control law is selected as

$$\bar{u}_j = \frac{1}{\alpha_{3j}} \{ -K_j \text{sat}(\hat{s}_j) + [k_{2j}/\epsilon_{oj} + c_{j1}(k_{1j}/\epsilon_{oj}) - (k_{1j}/\epsilon_{oj})^2] \tilde{x}_{1j} + \dot{x}_{1dj} - c_{j1}(\hat{x}_{2j} - \dot{x}_{1dj}) - \tilde{\Psi}_j \} \quad (37)$$

The resulting \hat{s}_j -dynamics including the effects of \tilde{x}_{2j} , becomes:

$$\dot{\hat{s}}_j = -K_j \text{sat}(\hat{s}_j) - (k_{1j}/\epsilon_{oj}) \tilde{x}_{2j}. \quad (38)$$

From the sliding conditions (7) the state estimation error is bounded by $|\tilde{x}_{2j}| \leq k_{1j}$. Therefore, in order to satisfy $\dot{\hat{s}}_j \hat{s}_j < 0$ outside the manifold $|\hat{s}_j| \leq \epsilon_{cj}$, the robust control gains must be chosen such that

$$K_j \geq k_{1j}^2/\epsilon_{oj}. \quad (39)$$

After the approaching phase, selection (39) assures $|\hat{s}_j| \leq \epsilon_{cj}$. Using $\tilde{s}_j = \hat{s}_j - s_j$ and Eqs. (23) (with $\text{sat}(\tilde{x}_{1j}) = \tilde{x}_{1j}/\epsilon_{oj}$), the actual s_j -dynamics within the boundary layer $|\hat{s}_j| \leq \epsilon_{cj}$ becomes

$$\dot{s}_j + \frac{K_j}{\epsilon_{cj}} s_j = \left[\frac{k_{2j}}{\epsilon_{oj}} - \left(\frac{k_{1j}}{\epsilon_{oj}} - \frac{K_j}{\epsilon_{cj}} \right) \left(c_{j1} - \frac{k_{1j}}{\epsilon_{oj}} \right) \right] \tilde{x}_{1j} - \left(c_{j1} + \frac{K_j}{\epsilon_{cj}} \right) \tilde{x}_{2j} - \tilde{\Psi}_j. \quad (40)$$

As we can see, the driving terms of s_j -dynamics are the estimation errors of the state and perturbations, which are bounded provided that the guidelines of Sections 3 and 4 are followed.

The details of the selection of the observer and controller parameters for a stable closed loop system are discussed next.

6 Design Procedure

This section proposes a systematic general design procedure considering the hardware limitations of the system. The purpose of this study is to provide some guidelines for the case of implementing SMCSPO in practical applications.

Once $|\tilde{x}_{1j}| \leq \epsilon_{oj}$ and $|\hat{s}_j| \leq \epsilon_{cj}$ are reached, i.e. the double sliding is in effect, observer and s_j dynamics take the form:

$$\begin{bmatrix} \ddot{\tilde{x}}_{1j} \\ \ddot{\tilde{x}}_{2j} \\ \ddot{\tilde{x}}_{3j} \\ \dot{s}_j \end{bmatrix} = \begin{bmatrix} -k_{1j}/\epsilon_{oj} & 1 & 0 & 0 \\ -k_{2j}/\epsilon_{oj} & \alpha_{3j}^2 & -\alpha_{3j} & 0 \\ 0 & \alpha_{3j} & -\alpha_{3j}^2 & 0 \\ k_{2j}/\epsilon_{cj} + (c_{j1} - k_{1j}/\epsilon_{oj})^2 - (2c_{j1} + \alpha_{3j}^2) & \alpha_{3j} & -c_{j1} & 0 \end{bmatrix} \begin{bmatrix} \tilde{x}_{1j} \\ \tilde{x}_{2j} \\ \tilde{x}_{3j} \\ s_j \end{bmatrix} + \begin{bmatrix} 0 \\ 0 \\ 1 \\ 0 \end{bmatrix} \dot{\Psi}_j/\alpha_{3j}, \quad (41)$$

where it is assumed that $c_{j1} = K_j/\epsilon_{cj}$ (same bandwidths for s_j and e_j dynamics). The selection of the parameters will be such that the poles of the system matrix in (41) are placed at desired and naturally stable locations. The associated characteristic equation is

$$[\lambda + c_{j1}][\lambda^3 + (k_{1j}/\epsilon_{oj})\lambda^2 + (k_{2j}/\epsilon_{oj})\lambda + \alpha_{3j}^2(k_{2j}/\epsilon_{oj})] = 0. \quad (42)$$

Let $p(\lambda_d) = (\lambda + \lambda_d)^4$ be the desired characteristic polynomial where, for simplicity, all the desired poles are selected to be at the same real valued location $\lambda = -\lambda_d$ ($\lambda_d > 0$). This leads to the following design solutions:

$$\begin{aligned} \frac{k_{1j}}{\epsilon_{oj}} &= 3\lambda_d \\ \frac{k_{2j}}{k_{1j}} &= \lambda_d \\ \alpha_{3j} &= \sqrt{\lambda_d/3} \\ c_{j1} &= K_j/\epsilon_{cj} = \lambda_d \end{aligned} \quad (43)$$

Ultimately, the transfer functions (28), (29), and (30) turn out to be

$$\tilde{\Psi}_j(p) = \frac{p(p^2 + 3\lambda_d p + 3\lambda_d^2)}{(p + \lambda_d)^3} (-\Psi_j(p)), \quad (44)$$

$$\tilde{x}_{2j}(p) = \frac{p(p + 3\lambda_d)}{(p + \lambda_d)^3} (-\Psi_j(p)), \quad (45)$$

$$\tilde{x}_{2j}(p) = \frac{p + 3\lambda_d}{p^2 + 3\lambda_d p + 3\lambda_d^2} (-\Psi_j(p)), \quad (46)$$

respectively. Figure 3 compares the magnitude plots of (45) (SPO) and (46) (SO). In this plot, the magnitudes are normalized with respect to the DC gain of (46) (i.e., $1/\lambda_d$). SPO clearly yields higher attenuation up to approximately $\omega/\lambda_d = 0.4$, meaning better estimation accuracy within this frequency range. If $0.4\lambda_d$ is placed much higher than the perturbation spectrum, then SPO is expected to outperform SO at any operating frequency. Note that for $\omega/\lambda_d > 0.4$ the discrepancy is minimal between the attenuation of SO and SPO, meaning close performance levels at high frequencies.

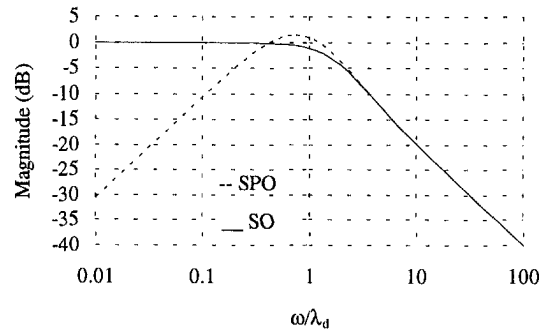


Fig. 3 Comparison of the magnitude plots of Eqs. (45) and (46) normalized by λ_d

Physical limitations of the control system define the optimum placement of λ_d . Some examples of such hardware constraints are: sampling frequency, measurement delay and actuator dynamics. Consider τ^{hw} to be the dominant time delay in the hardware. This is an a priori known quantity and it can be experimentally determined. Once $|\tilde{x}_{1j}| \leq \epsilon_{oj}$ the observer sliding mode dynamics become $\dot{\tilde{x}}_{1j} + (k_{1j}/\epsilon_{oj})\tilde{x}_{1j} = \tilde{x}_{2j}$ (as indicated by (41)), which is a filter with input \tilde{x}_{2j} , output \tilde{x}_{1j} (the observer sliding function) and break point k_{1j}/ϵ_{oj} . It is shown in Moura et al. (1995) that the break point of the sliding function dynamics inside a manifold cannot exceed $1/(5\tau^{hw})$. Similar proposition is also presented in Slotine and Li (1991). Therefore, according to the first of Eqs. (43) the best selection of λ_d is

$$\lambda_d = \frac{1}{15\tau^{hw}}. \quad (47)$$

This simple entity defines the necessary SPO parameters via (43) based on the limitation of the hardware at hand.

7 SMCSPO Versus Full State Feedback SMC

This section presents a comparison between SMCSPO with partial state feedback versus conventional SMC with full state feedback and no measurement noise. The tool for comparison is the transfer function that relates s_j and Ψ_j in each algorithm. The higher the attenuation within the perturbation spectrum, the better the performance of the algorithm.

7.1 $s_j(p)/\Psi_j(p)$ for SMCSPO. Using (40), (43)–(45) and the sliding property that $\tilde{x}_{1j}(p) = \tilde{x}_{2j}(p)/(p + k_{1j}/\epsilon_{oj})$, the frequency domain relation between s_j and Ψ_j for SMCSPO is

$$s_j(p) = \frac{(p^2 + 5\lambda_d p + 10\lambda_d^2)p}{(p + \lambda_d)^4} \Psi_j(p). \quad (48)$$

7.2 $s_j(p)/\Psi_j(p)$ for SMC With Full State Feedback and Perfect Measurements. For the dynamics of Eq. (1), it is shown in Slotine and Sastry (1983) and Elmali and Olgac (1992) that conventional SMC, after the approaching phase, yields

$$s_j + \frac{K_j}{\epsilon_{cj}} s_j = \Psi_j \quad (49)$$

where $K_j \geq |\Psi_j|$ (upper bound of perturbations) is selected in order to assure that $|s_j| \leq \epsilon_j$ is maintained. The driving terms in Eq. (49) are the perturbations, as opposed to the state and perturbation estimation errors in Eq. (40). In both cases K_j/ϵ_{cj} is the break frequency which is set equal to λ_d for a fair comparison with SMCSPO. $K_j/\epsilon_{cj} = \lambda_d$ proposition is also used to determine the variable boundary layer ϵ_{cj} . With this substitution, Eq. (49) takes the form

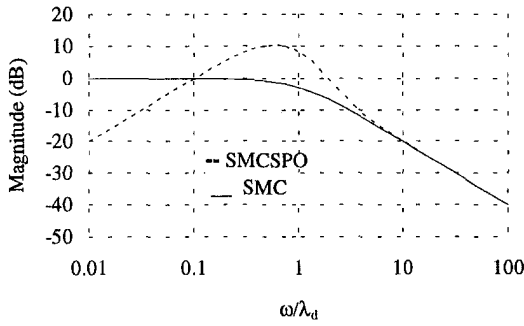


Fig. 4 Normalized magnitude plots of SMC and SMCSPO $s_j(\omega)/\Psi_j(\omega)$ transfer functions

$$s_j(p) = \frac{1}{p + \lambda_d} \Psi_j(p), \quad (50)$$

Figure 4 compares the magnitude plots of $s_j(p)/\Psi_j(p)$ for SMC and SMCSPO. Both plots are normalized with respect to the DC gain of (50). For high frequency contents of Ψ_j , both algorithms behave the same. In the mid-frequency range, the maximum discrepancy is about 10 dB in favor of SMC. In smaller frequencies, however, SMCSPO outperforms SMC up to a designer selected frequency $\lambda_\Psi = 0.1\lambda_d$, which can be set to a higher value than the most expected frequency components of the perturbations. It is important to note that the SMC considered here needs full state feedback and no measurement noise. On the other hand, SMCSPO utilizes only partial state feedback, nonetheless SMCSPO still exhibits superior performance.

We wish to draw the attention to some extra terms like $\tilde{f}_j = f_j(\hat{\mathbf{x}}) - f_j(\mathbf{x})$ and $\tilde{b}_{ji} = b_{ji}(\hat{\mathbf{x}}) - b_{ji}(\mathbf{x})$ in the perturbation estimation of SMCSPO. They appear due to the state estimation errors. Consequently, the perturbation signal, Ψ_j , may have large magnitudes which are not desirable. The influence of \tilde{f}_j and \tilde{b}_{ji} on s_j , however, can be made negligible. To achieve this one should revisit the filter of (48). It is easy to observe that the filter attenuation at frequency λ_d is $-20 \log \lambda_d + 10$ dB. That is, as long as $\lambda_d \geq 3.2$ rad/s, the influence of these estimation error terms on s_j is negligible. Another practical observation is that, for applications such as motion control of multi-arm articulated mechanisms, the matrix $\mathbf{B} = [b_{ji}(\mathbf{x})]$ is the inverse of the inertia matrix, thus it depends only on joint positions (i.e., angles or translations), which makes $b_{ji} = 0$ for this particular application when the position feedback is available.

Figure 5 depicts the closed loop dynamics of SMC and SMCSPO in block diagrams. In both cases, the perturbations are filtered yielding tracking errors as the output. The perturbation estimation attenuates the effects of the perturbation signal. Note that SMC strategy cannot eliminate DC offsets in the perturbation signal, as opposed to SMCSPO which yields infinite attenuation at zero frequency. Therefore, if the uncertainties contain

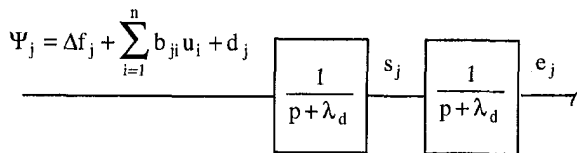


Fig. 5(a) Block diagram of SMC strategy

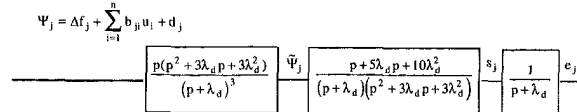


Fig. 5(b) SMCSPO strategy

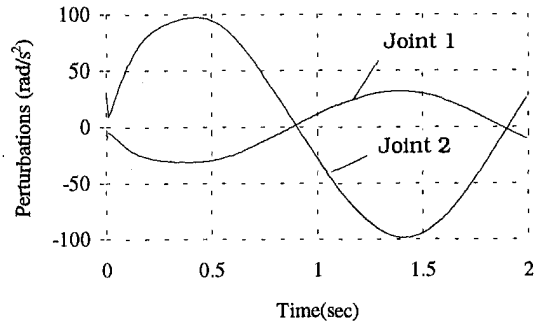


Fig. 6 Actual perturbations, Joints 1 and 2

some constant offset (e.g. gravity or dry friction) then SMCSPO will remove its influence completely on the tracking error, which is not possible with SMC routine. Strategies such as Integral Sliding Mode [Cho et al., 1993] are developed to eliminate this bias requiring a modification in the sliding function.

8 Simulations

This section presents simulation results using a two-link SCARA type manipulator in order to verify Eqs. (45) and (48). Performance evaluation and experimental comparisons with other techniques are left to the next section. The actual manipulator model is taken as (Moura et al., 1995):

$$\begin{bmatrix} \ddot{\theta}_1 \\ \ddot{\theta}_2 \end{bmatrix} = \mathbf{I}^{-1} \begin{bmatrix} u_1 - b_{v1}\dot{\theta}_1 + m_2 l_1 l_{g2} \sin(\theta_2)(\dot{\theta}_2^2 + \dot{\theta}_1 \dot{\theta}_2) \\ u_2 - b_{v2}\dot{\theta}_2 - m_2 l_1 l_{g2} \sin(\theta_2)\dot{\theta}_1^2 \end{bmatrix} \quad (51)$$

where $\mathbf{I} = \begin{bmatrix} I_{11} & I_{12} \\ I_{21} & I_{22} \end{bmatrix}$ is the inertia matrix, $I_{11} = I_1^0 + m_1 l_{g1}^2 +$

$m_2 l_1^2 + I_2^0 + m_2 l_{g2}^2 + 2m_2 l_1 l_{g2} \cos(\theta_2)$, $I_{12} = I_2^0 + m_2 l_{g2}^2 + m_2 l_1 l_{g2} \cos(\theta_2) = I_{21}$, $I_{22} = I_2^0 + m_2 l_{g2}^2$, u_j = control torque; $b_{v,j}$ = viscous friction coefficients ($j = 1, 2$); I_j^0 = joint j moment of inertia with respect to its center of mass ($j = 1, 2$). In this model, the links are taken as slender rods with mass concentrated at the mid-point, yielding $I_j^0 = m_j l_j^2 / 12$. The numerical parameters are: $l_1 = 0.3$ m = $2l_{g1}$; $l_2 = 0.3$ m = $2l_{g2}$; $m_1 = 5.0$ Kg; $m_2 = 5.0$ Kg; $b_{v1} = b_{v2} = 5.5$ Ns.

In this simulation, the perturbations are assumed to entail friction forces, coriolis and centrifugal acceleration terms. The control task consists of tracking $\theta_{1d} = (\pi/18) \sin(\pi t/2)$ rad and $\theta_{2d} = (\pi/18) \cos(\pi t/2)$ rad. The state vector is chosen as $[\theta_1 \ \dot{\theta}_1 \ \theta_2 \ \dot{\theta}_2]^T$.

The control loop is closed at 1 KHz sampling rate. It is assumed that the sampling period is the dominant time delay of the closed-loop system. The parametric selections for SMCSPO algorithm follow the design of Section 6.

Figure 6 depicts the actual perturbations for the first two seconds of the simulation. The dominant frequency is identical to that of the desired motion. After the simulations are finished, the signals of Fig. 6 are fed through the filter of Eq. (45) and the output is compared with the actual velocity estimation errors. This procedure is repeated for each joint. The results are depicted in Fig. 7. It is clear that Eq. (45) correctly describes the estimation error dynamics. The small discrepancy within the first 0.1 in Fig. 7(a) is due to the filter transients, which disappear at steady state.

Figure 8 depicts the results regarding Eq. (48). Similar to Fig. 7, the predicted sliding functions were obtained by feeding the actual perturbation signal of Fig. 6 through the filter of Eq. (48). The resulting outputs were plotted together with the actual sliding functions of the respective joint. Obviously the predictions of Eq. (48) are verified by these plots. Again a small discrepancy is noticed in Fig. 8(a) due to the filter transients.

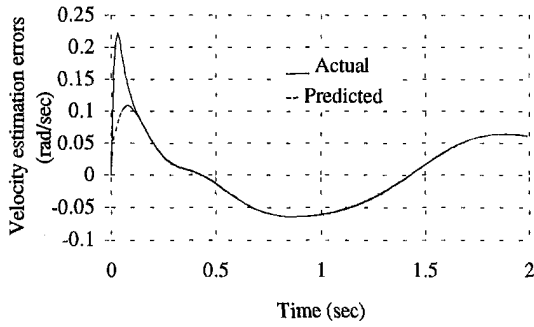


Fig. 7(a) Joint 1

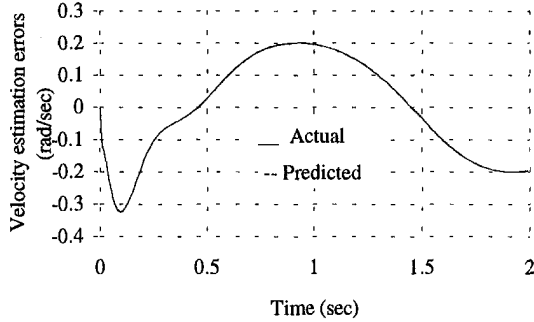


Fig. 7(b) Joint 2

Fig. 7 Actual and predicted velocity estimation errors

9 Experimental Results

This section presents experimental results of SMCSPO algorithm. The controlled system is a PUMA 560 robotic manipulator (Yoshikawa, 1990) of which the first 3 links are considered only. For comparison purposes, two full state feedback algorithms are also tested: conventional SMC and Computed Torque Method (CTM) (Yoshikawa, 1990). The algorithms are imple-

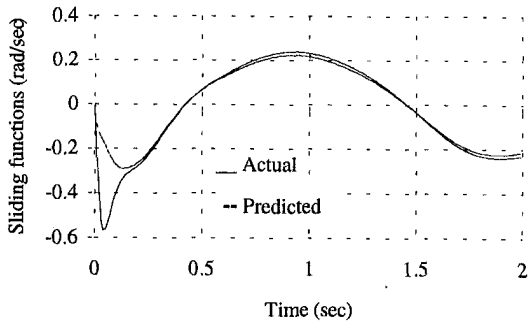


Fig. 8(a) Joint 1

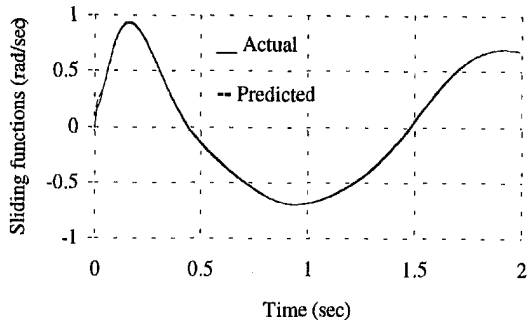


Fig. 8(b) Joint 2

Fig. 8 Actual and predicted sliding functions from Eq. (40)

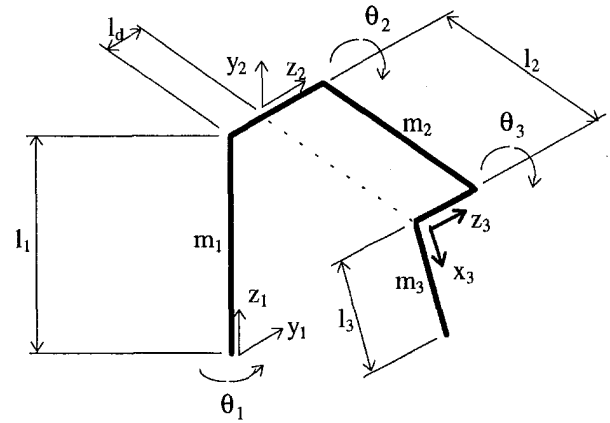


Fig. 9 Simplified model of the manipulator used by the algorithms

mented on a 80486/50 MHz CPU. The source code is written in C. DC motors (with 0.264 Nm/amp) provide the joint actuation. The gear ratios for joints 1, 2 and 3 are 62.6, 107.8 and 53.7, respectively. Digital encoders with 5000 counts/rev are utilized for joint angle measurements, tachometers generate the joint velocity signals (7 Volts/1000 RPM with 5 percent ripple) for SMC and CTM.

The simplified manipulator model used by all those algorithms is

$$\ddot{\theta} = \mathbf{B}\mathbf{u} \quad (52)$$

where \mathbf{u} is the vector of the control torques, $\mathbf{B} = \mathbf{I}^{-1}$ and \mathbf{I} is the inertia matrix. This matrix is obtained modeling the three links as slender rods with the center of mass located at their mid points, as shown in Fig. 9. Equation (52) ignores viscous and coulomb friction, coriolis terms, external loads, payloads and an accurate description of the mass distribution of the links. All of these uncertainties are included in the perturbation vector. The components of the inertia matrix $\mathbf{I} = [I_{ij}]$, ($i, j = 1, 2, 3$) are computed as:

$$I_{11} = I_{z_1} + m_2(l_d^2 + 0.25l_2^2 \cos^2(\theta_2)) + I_{x_1} \sin^2(\theta_2) + I_{y_2} \cos^2(\theta_2) + m_3(l_2 \cos(\theta_2) + l_3 \cos(\theta_2 + \theta_3)/2)^2 + I_{x_3} \sin^2(\theta_2 + \theta_3) + I_{y_3} \cos^2(\theta_2 + \theta_3)$$

$$I_{22} = m_2 l_2^2 / 4 + I_{z_2} + m_3(l_2^2 + l_2 l_3 \cos(\theta_3) + l_3^2 / 4) / 2 + I_{z_3}$$

$$I_{33} = I_{z_3} + m_3 l_3^2 / 4$$

$$I_{12} = I_{21} = l_d \{ m_3 [l_2 \sin(\theta_2) + l_3 \sin(\theta_2 + \theta_3) / 2] / 2 - m_2 l_2 \sin(\theta_2) / 2 \}$$

$$I_{13} = I_{31} = m_3 l_d l_3 \sin(\theta_2 + \theta_3) / 2$$

$$I_{23} = I_{32} = m_3 [l_3^2 / 4 + l_2 l_3 \cos(\theta_3) / 2] + I_{z_3}$$

where $I_{\alpha i} = m_i l_i^2 / 12$ is the moment of inertia of link i about axis α which goes through the center of gravity of the link. θ_1 , θ_2 , and θ_3 are the joint angles taken relative to the previous link. The corresponding numerical values of the manipulator parameters are: $m_1 = 12.95$ Kg, $m_2 = 22.36$ Kg, $m_3 = 5.0$ Kg, $l_1 = 0.673$ m, $l_2 = 0.432$ m, $l_3 = 0.434$ m and $l_d = 0.08$ m.

SMC control law uses (for details see Slotine and Sastry, 1983 and Elmali and Olgac, 1992):

$$\mathbf{u} = \mathbf{I}[-\mathbf{K} \text{sat}(\mathbf{s}) - \dot{\mathbf{c}} + \ddot{\theta}_d] \quad (53)$$

where $\mathbf{K} = \text{diag}[K_j]$ ($K_j > 0$), $\text{sat}(s) = [\text{sat}(s_1) \dots \text{sat}(s_n)]^T$, $\mathbf{c} = \text{diag}[c_{j1}]$, $\dot{\mathbf{c}} = [\dot{c}_1 \dots \dot{c}_n]^T$ and $\theta_d = [\theta_{1d} \dots \theta_{nd}]^T$ is the desired motion vector. In order to assure $|s_j| \leq c_{c_j}$ in steady state the control gains must be selected as

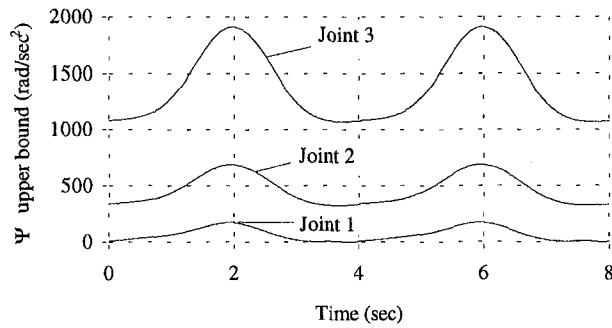


Fig. 10 Upper bounds of the perturbations for PUMA manipulator

Table 1 Parameter selections of all strategies— $j = 1, 2$

| Algorithm | Parameters |
|-----------|--|
| SMCSPO | $k_{o1j}/\epsilon_{o1j} = 150$ rad/s; $k_{o2j}/k_{o1j} = 50$ rad/s; $\alpha_{3j} = \sqrt{50/3}$ rad/s; $K_j/\epsilon_{c_j} = 50$ rad/s; $c_j = 50$ rad/s |
| SMC | $K_j/\epsilon_j = c_j = 50$ rad/s |
| CTM | $K_{pj} = 2500$ sec ⁻² ; $K_{vj} = 100$ s ⁻¹ |

$K_j > |\Psi_j|$ according to Eq. (3). The control (53) yields the s_j -dynamics of Eq. (49).

The CTM utilizes the following control law (Yoshikawa, 1990):

$$\mathbf{u} = \mathbf{I}[\ddot{\theta}_d - \mathbf{K}_p \mathbf{e} - \mathbf{K}_v \dot{\mathbf{e}}] \quad (54)$$

where $\mathbf{K}_p = \text{diag}[K_{pj}]$, $\mathbf{K}_v = \text{diag}[K_{vj}]$ are the proportional and derivative gain matrices, respectively.

The parameters of SMC and CTM are selected such that the resulting tracking error dynamics possess the same desired poles as in SMCSPO (i.e., λ_d). This makes it possible to have a fair performance comparison between all the presented algorithms. For SMC, the tracking error dynamics is obtained using Eq. (50). The final result gives:

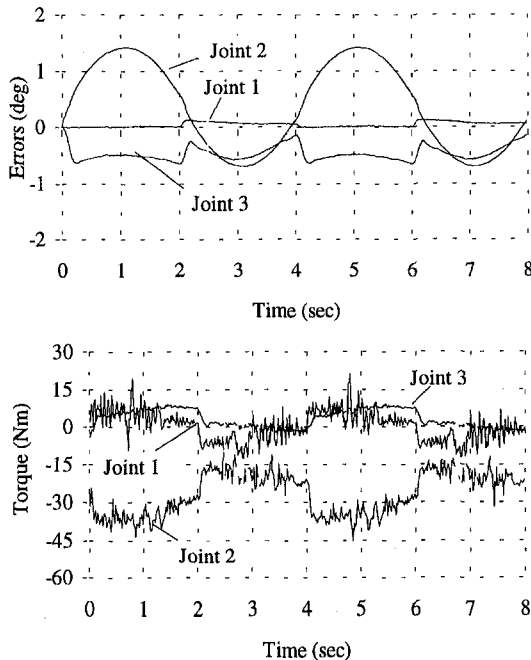


Fig. 11 Computed Torque Method. Position tracking errors and control torques.

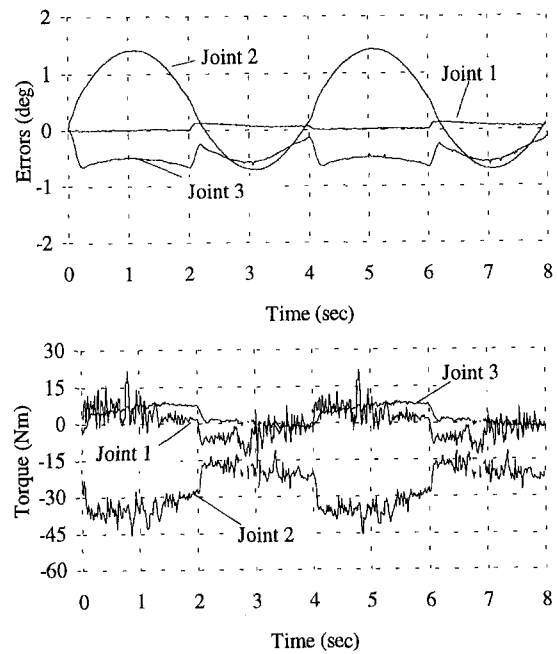


Fig. 12 Sliding Mode Control. Position tracking errors and control torques.

$$e_j(p) = \frac{1}{(p + c_{j1})(p + \lambda_d)} \Psi_j(p). \quad (55)$$

Therefore our selection is $c_{j1} = \lambda_d$. For the CTM the closed-loop dynamics yield:

$$e_j(p) = \frac{1}{p^2 + K_{vj}p + K_{pj}} \Psi_j(p). \quad (56)$$

Therefore, the gains are selected as $K_{vj} = 2\lambda_d$ and $K_{pj} = \lambda_d^2$ so that the characteristic polynomial has all the roots at $-\lambda_d$. The selections for SMCSPO are given in (43).

The experiments are carried out on the PUMA 560 robot for the following desired trajectory:

$$\theta_{jd} = 0.34[1 - \cos(\pi t/2)] \text{ rad} \quad j = 1, 2, 3 \quad (57)$$

The upper bounds of the perturbations are calculated based on the PUMA 560 dynamic model proposed by Armstrong et al. (1986). The perturbations consist of coriolis and centrifugal terms, gravity effect, viscous and Coulomb friction forces and uncertainties in the inertia matrix. For our experimental setup the following assumptions are made: $|\Delta b_{ji}| \leq 0.5|b_{ji}|$ ($j, i = 1, 2, 3$), the viscous friction coefficients in all the joints are less than 40 Nms, the Coulomb friction coefficients are all less than 3 Nm and the applied control torques do not exceed 50 Nm for the desired motion. Using the desired state to compute the state dependent terms and the worst case scenario for uncertainties, the perturbation upper bounds can be computed from Eq. (3) using: $|\Phi_{ji}(\theta_d)u_i| = |0.5b_{ji}(\theta_d)(50)|$, $D_j(\dot{\theta}_{jd}) = 3 \text{ sign}(\dot{\theta}_{jd}) + 40\dot{\theta}_{jd} + g_j(\theta_d)$, where g_j is the gravity effect and the term $F_j(\theta_d, \dot{\theta}_d)$ (from (3)) represents the coriolis and centrifugal terms of the PUMA 560 as described in details in Armstrong et al. (1986). The resulting expected perturbation upper bounds are plotted in Fig. 10. Based on these results, 500 rad/s², 1000 rad/s² and 2000 rad/s² are selected as the robust gains of SMC and SPO for joints 1, 2, and 3, respectively.

In the experimental setup utilized, the control sampling speed (600 Hz) and the actuator time constants ($\cong 1$ ms) are the major causes of time delay in the control loop. The former is clearly the dominant. In order to prevent this hardware imposed bound to be an influential point in our comparisons, we set λ_d

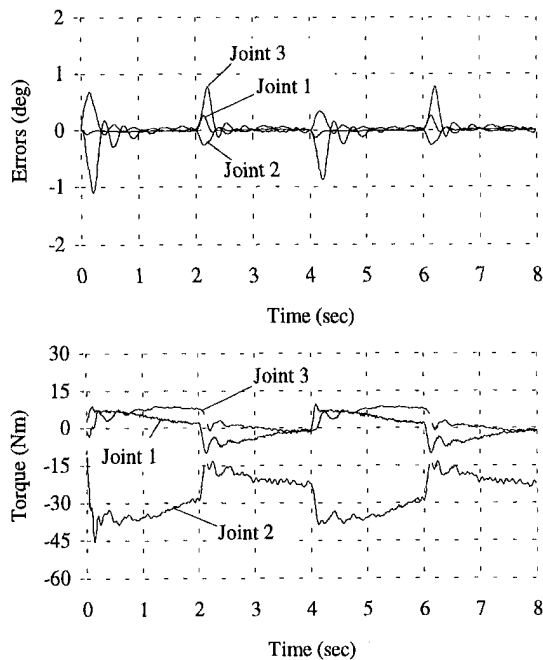


Fig. 13 SMCSPO—position tracking errors and control torques

= 50 rad/sec ($\cong 8$ Hz) for all the control strategies. Table 1 depicts these parameters selections.

The position tracking errors for CTM, SMC, and SMCSPO are depicted in Figs. 11(a), 12(a), and 13(a), respectively. The results of CTM and SMC are almost identical. The reason for this is the fact that the control laws (53) and (54) become identical when the sliding regime is obtained (for the selected closed loop poles). SMCSPO is able to provide a superior performance over CTM and SMC. The peak errors in SMCSPO occur whenever the velocity sign changes. At these instants, Coulomb friction becomes discontinuous and $\dot{\Psi}_j$ terms get very large. Therefore it is expected a poor estimation performance of the SPO. The overall tracking accuracy of SMCSPO is at least one order of magnitude better than the other two algorithms. Note the presence of a DC offset in all the plots of CTM and SMC, but not in SMCSPO. This bias is due to the gravity effect which appears in all the joints through the dynamic coupling. Also, the signals depicted in Figs. 11(a) and 12(a) contain significant presence of the desired motion frequency, which reflects the spectrum of the perturbations. On the other hand, SMCSPO strategy is able to filter the influence of the perturbations much more effectively, as predicted by the theory. The control torques are depicted in Figs. 11(b), 12(b), and 13(b). Note that SMCSPO is able to achieve better performance with less control activity. The reason for that is the presence of noise (5 percent ripple) in the velocity feedback which appears in

both SMC and CTM. SMCSPO utilizes only position feedback which is performed by digital encoders and thus almost error free.

10 Conclusions

This work introduces a new robust tracking control algorithm named Sliding Mode Control with Sliding Perturbation Observer for a general class of second order nonlinear systems. The consolidation of the SPO into the SMC routine demonstrates significant performance improvement over the full state feedback form of the SMC. The proposed observer also proves to be superior than conventional sliding observers due to the perturbation estimation feature. The stability analysis shows that as long as the observer stability is guaranteed, the controller can be also made stable. A detailed design procedure for a systematic formulation of the new routine is presented utilizing frequency domain techniques. Verification of the analytical proposition is presented via simulation examples. The performance of SMCSPO is shown to be limited by the dominant time constant of the control process. Experiments on a 3 axis PUMA 560 manipulator confirms the superior performance of SMCSPO over two well known motion control techniques, the conventional SMC and CTM. Further research will include: a better design of the perturbation estimator in order to expand the frequency range where SMCSPO outperforms SMC; and to identify engineering applications where SMCSPO can offer substantial improvement over state of the art techniques.

Acknowledgments

The first author wishes to thank the Brazilian government for the partial financial support under the process CNPq 200350/92-7. The second and third authors express their appreciation for the NSF grant CMS 9415428.

References

- Elmali, H., and Olgac, N., 1992, "Sliding Mode Control with Perturbation Estimation (SMCPE): A New Approach," *International Journal of Control*, Vol. 56, pp. 923–941.
- Ježernik, K., Curk, B. and Harnik, J., 1994, *Variable Structure and Lyapunov Control*, Alan Zinober, ed., Chapter 18, pp. 389–400, Springer-Verlag, New York.
- Luenberger, D. G., 1965, "Observing the State of a Linear System," *IEEE Transactions on Military Electronics*, Apr., pp. 74–80.
- Moura, J. T., Roy, R. and Olgac, N., 1995, "Sliding Mode Control with Perturbation Estimation (SMCPE) and Frequency Shaped Sliding Surfaces," 1995 ASME International Mechanical Engineering Congress and Exposition, San Francisco, CA, Nov.
- Slotine, J. J., Hedrick, J. K., Misawa, E. A., 1987, "On Sliding Observers for Non-Linear Systems," *ASME JOURNAL OF DYNAMIC SYSTEMS, MEASUREMENT, AND CONTROL*, Vol. 109, pp. 245–252, Sept.
- Slotine, J. J. and Li, W., 1991, *Applied Nonlinear Control*, Prentice-Hall.
- Slotine, J. J. and Sastry, S. S., 1983, "Tracking Control of Non-linear Systems Using Sliding Surfaces with Application to Robot Manipulators," *International Journal of Control*, Vol. 38, pp. 465–492.
- Yoshikawa, T., 1990, *Foundations of Robotics Analysis and Control*, MIT Press.
- Armstrong, B., Khatib, O. and Burdick, J., 1986, "The Explicit Dynamic Model and Inertial Parameters of the PUMA 560 Arm," *Proceedings of the IEEE Conference on Robotics and Automation*, Vol. 1, pp. 510–518, April 7–10, San Francisco, CA.